Original Article

A method for separating and quantifying organic and inorganic ice nucleating substances in atmospheric samples based on density gradient centrifugation

Soleil E. Worthy[a], Lanxiadi Chen[b,c], Gurcharan K. Uppal[a], Yu Xi[a], Vakshan Varatharajah[a], Marie Line Torrijos[d], Anne Fuertes[a], Runqiu Song[a], Qianqian Zhang[a], Joyce Huang[a], and Allan K. Bertram[a]

[a]Department of Chemistry, University of British Columbia, Vancouver, British Columbia, Canada; [b]State Key Laboratory of Organic Geochemistry and Guangdong Key Laboratory of Environmental Protection and Resources Utilization, Guangzhou Institute of Geochemistry, Chinese Academy of Sciences, Guangzhou, China; [c]College of Earth and Planetary Sciences, University of Chinese Academy of Sciences, Beijing, China; [d]Department of Chemistry, Sorbonne University, Paris, France

CONTACT Allan K. Bertram bertram@chem.ubc.ca Department of Chemistry, University of British Columbia, Vancouver, BC, V6T 1Z1, Canada.

ABSTRACT

Ice nucleating substances (INSs) influence the properties and frequencies of ice and mixed-phase clouds in the atmosphere, and hence, climate and the hydrological cycle. INSs can be classified as inorganic (e.g., mineral dust, volcanic ash) or organic (e.g., bacterial cells, cell-free proteins). While the properties of both INS classes have been studied in the laboratory, the amounts in the atmosphere are still poorly constrained. Here, we demonstrate a new method for separating and quantifying inorganic and organic INSs. First, INS suspensions were separated into a high-density isolate containing inorganic INSs and a low-density isolate containing organic INSs using density gradient centrifugation, and then INSs were quantified in each isolate using a droplet freezing technique. Inorganic K-feldspar and organic Snomax INSs were used to test our method. The average K-feldspar INS recovery in the high-density isolate was 54%, with no evidence of K-feldspar INSs in the low-density isolate. The average Snomax INS recovery in the low-density isolate was 27%, with small amounts of Snomax contaminating the high-density isolate. A mixture of K-feldspar and Snomax was successfully separated, with recoveries comparable to those observed for K-feldspar and Snomax individually. Recoveries less than 100% can be explained by losses of INSs to vessel walls, accidental mixing of the different density layers during pipetting, and incomplete collection of material during pipetting.

1. Introduction

In the atmosphere, ice can form homogeneously at temperatures $\lesssim$ -35 °C (Koop and Murray 2016). Alternatively, ice can form heterogeneously in the atmosphere at temperatures > -35 °C when ice nucleation is initiated by an ice nucleating substance (INS) (Hoose and Möhler 2012; Kanji et al. 2017; Murray et al. 2012). There are several different modes of heterogeneous ice nucleation including immersion freezing, deposition nucleation, pore-condensation freezing, and contact freezing (David et al. 2019; Vali et al. 2015). Immersion freezing, which is the focus of our study, occurs when freezing is initiated by an INS immersed in an aqueous droplet and can dominate ice formation in mixed-phase clouds (Ansmann et al. 2009; Vali et al. 2015; Westbrook and Illingworth 2013). INSs allow for the formation of ice crystals in clouds at warmer temperatures and lower water vapor pressures than those required for homogenous ice nucleation. As a result, INSs affect cloud properties and therefore the climate via effects on the hydrological cycle and Earth's radiative properties (Boucher et al. 2013; Lohmann 2002; Lohmann and Feichter 2005; Tan, Storelvmo, and Zelinka 2016).

INSs can be divided into organic and inorganic substances. Inorganic INSs include mineral dusts, volcanic ash, metals, and metal oxides, with mineral dust being a particularly prevalent class of inorganic INSs in the atmosphere (Burrows et al. 2022; Kanji et al. 2017). Organic INSs include a wide range of materials such as bacterial cells, fungal and pollen spores, cell-free biomolecules such as proteins or polysaccharides, humic-like substances, secondary organic aerosols, and biomass burning aerosols (Burrows et al. 2022; Dreischmeier et al. 2017; Kanji et al. 2017; Knopf, Alpert, and Wang 2018; Pummer et al. 2015). The properties of both organic and inorganic INSs have been studied in the laboratory, but the absolute and relative amount of organic and inorganic INSs in the atmosphere remains poorly constrained, leading to uncertainties when predicting mixed-phase and ice clouds in the atmosphere. (Burrows et al. 2022; Dreischmeier et al. 2017; Kanji et al. 2017; Knopf, Alpert, and Wang 2018; Pummer et al. 2015).

Several methods are available for quantifying the absolute and relative amounts of organic and inorganic INSs in the atmosphere. One approach involves single-particle analysis combined with methods of isolating INSs. Methods for analyzing isolated INSs include single-particle mass spectrometry (Burrows et al. 2022; Corbin et al. 2012; Cziczo et al. 2004; DeMott et al. 2003; Pratt et al. 2009) and single-particle microscopy (Burrows et al. 2022; Iwata and Matsuki 2018; Knopf et al. 2010; Knopf et al. 2022; Prenni et al. 2009). Although these methods offer invaluable insights, they can suffer from poor sampling statistics and require specialized operators and specialized and expensive equipment. As a result, these techniques are not accessible to many laboratories.

Another class of techniques that can be used to quantify the absolute and relative amounts of organic and inorganic INSs in atmospheric samples involves treating atmospheric samples with H_2O_2, heat, or $(NH_4)_2SO_4$ and observing the change in ice nucleating efficiency due to the treatment. H_2O_2 treatment is used to remove organic material. H_2O_2 can be used to quantify organic and inorganic INSs in atmospheric samples by measuring the concentration of INSs before and after H_2O_2 treatment with standard freezing assays (Conen et al. 2011; Hill et al. 2016). Heat treatment has been used to denature heat-active proteins (a type of organic INSs). Heat treatment can be used to quantify protein INSs in atmospheric samples by measuring the concentration of INSs before and after heat treatment (Christner et al. 2008; Irish et al. 2019; O'Sullivan et al. 2014; Schnell and Vali 1975; Wilson et al. 2015). $(NH_4)_2SO_4$ treatment is used to enhance the freezing properties of mineral dust (a type of inorganic INSs) (Kumar et al. 2018; Kumar, Marcolli, and Peter 2019a; Kumar, Marcolli, and Peter 2019b; Whale et al. 2018; Worthy et al. 2021). The presence of mineral dust INSs can be detected in atmospheric samples by measuring the concentration of INSs before and after treatment with $(NH_4)_2SO_4$ via a standard freezing assay (Worthy et al. 2021; Xi et al. 2022; Yun et al. 2022). However, H_2O_2, heat, and $(NH_4)_2SO_4$ treatments are susceptible to overestimating or underestimating the contributions of INSs of interest as the treatments may affect INSs in the sample other than the target INSs or may not affect all of the target INSs (Daily et al. 2022; Perkins et al. 2020). For the

aforementioned reasons, additional techniques are needed to better detect and quantify organic and inorganic INSs.

One property of organic INSs that differs significantly from inorganic INSs is density (Table S1). Organic INSs generally have densities of 1.6 g cm^{-3} or less (Anderson et al. 1966; Bakken and Olsen 1983; Bratbak and Dundas 1984; Dinar, Mentel, and Rudich 2006; Durham 1943; Harding 1992; Harrington and Metzger 1963; Inoue et al. 2007; Neurohr, Amon, and Koch 2020; van Hout and Katz 2004), whereas inorganic INSs have densities of 2.1 g cm^{-3} or greater (Anthony et al. 2001; Bagheri and Bonadonna 2016; Hazardous Substances Data Bank (HSDB) 2023; National Center for Biotechnology Information 2023; Saxby et al. 2018; Vogel et al. 2017; Wintle 1997; Woor et al. 2022). Here, we present a new method for separating and quantifying organic and inorganic INSs based on density gradient centrifugation, which takes advantage of these differences. This method is straightforward and uses instruments that are available in many laboratories. This method should also be compatible with INS samples collected using filters or impingers (Schneider et al. 2021; Schrod et al. 2020). Additionally, this method does not suffer from sampling statistics since many samples can be processed in a reasonable amount of time (Knopf and Alpert 2013).

Density gradient centrifugation is a well-established technique and has been previously used for a wide variety of separations including the separation of organic particles from inorganic particles in soil, natural waters, and pond sediments (Backman and Jansson 2004; Bakken 1985; Lammers 1963; Lindahl and Bakken 1995). Nevertheless, the technique has not been used previously to separate or characterize INSs.

Below, we describe in detail our method for separating and quantifying organic and inorganic INSs via density gradient centrifugation and a droplet freezing technique. We then present several experiments used to test the efficacy of this approach. These experiments are aimed at answering several questions: 1) Does the method introduce INSs into the low- and high-density isolates? 2) Does the density gradient medium influence the freezing properties of the INSs? 3) What percentage of inorganic INSs can this method recover

in the high-density isolate and do any inorganic INSs contaminate the low-density isolate? 4) What percentage of organic INSs can this method recover in the low-density isolate and do any organic INSs contaminate the high-density isolate? This information will allow us to better assess the potential performance and suitability of this method for use on atmospheric samples and identify any areas for possible improvements. These experiments were carried out with potassium-rich feldspar as the test inorganic INS and Snomax as the test organic INS.

2. Materials and methods

Our experimental method consists of first separating an INS suspension into a low-density fraction and high-density fraction using density gradient centrifugation (Section 2.1). The low- and high-density fractions are then washed via differential centrifugation to remove density gradient medium from the INSs (Section 2.2). The concentration of INSs in the two isolates are then quantified with the droplet freezing technique (Section 2.3).

2.1. Density gradient centrifugation

Density gradient centrifugation is a technique that involves separating material in a solution on the basis of buoyant density. For our experiments, a sample of interest is layered on top of a medium of known density (density gradient medium) and centrifuged. Any material present in the sample with a density greater than that of the density gradient medium should migrate through the density gradient medium under the centrifugal force, forming a pellet at the bottom of the experimental vessel, as long as sufficient sedimentation time is provided. Any material less dense than the density gradient medium should not be able to pass through the medium, no matter how long centrifugal force is applied. This separates the sample into two fractions: one with material less dense than the density gradient medium, and one with material more dense than the density gradient medium (Figure 1, steps 1-2).

Figure 1

Our density gradient centrifugation method was loosely based on the method developed by Lindahl and Bakken (1995) for the separation of soil particles and soil bacteria. First, 5 mL of OptiPrep™ density gradient medium (STEMCELL Technologies, Cat #07820) was placed in the bottom of a 15 mL centrifuge tube. OptiPrep™ is a non-ionic, non-toxic to cells, isosmotic, and metabolically inert medium consisting of 60% w/v iodixanol (molecular weight = 1550 g/mol). OptiPrep™ has a density of 1.320 ± 0.001 g cm^{-3} as specified by the manufacturer. Next, a 500 µL layer of ultrapure water was carefully placed on top of the density gradient medium followed by 750 µL of INS suspension, taking great care to avoid any mixing between layers (Figure 1, step 1). This water layer was placed between the density gradient medium and the INS suspension to prevent mixing between the two when pipetting. Ultrapure water is defined herein as distilled water purified by a Milllipore system to a resistivity of 18.2 M Ω cm at 25 °C. The tube was then centrifuged at 3,214 × g for 2 hours in an Eppendorf S-4-104 swing-bucket rotor (Figure 1, step 2). Calculations confirm that the centrifugal force and time used in our experiments should be sufficient for inorganic particles of densities ≥ 2.5 g cm^{-3} and sizes of ≥ 0.23 µm to pass through the 5 mL OptiPrep™ cushion (see SI, Section 1, Table S2).

After centrifugation, the total volume of low-density material above the density gradient medium cushion (~1250 µL) was collected via micropipette (Figure 1, step 3). The micropipette tip was held at the interface of the low-density water and density gradient medium during pipetting since the majority of our organic INSs should have collected at this interface. The density gradient medium cushion was then removed and discarded, except for approximately 50-100 µL of density gradient medium at the bottom of the centrifuge tube, which should contain any high-density material in the form of a pellet (Figure 1, step 3). This remaining 50-100 µL density gradient medium and any high-density material was resuspended in 50 µL of ultrapure water, transferred to a clean vessel, and then 1200 µL of ultrapure water were added to bring the total volume to between 1300 and 1350 µL (Figure 1, step 4).

In the current experiments, we used K-feldspar and Snomax as test INSs. Considering our use of OptiPrep™ (density of 1.320 g cm^{-3}) as the density gradient medium, we expect K-feldspar, which has a density of 2.55 – 2.63 g cm^{-3}, to pass through the density gradient medium and form a pellet. We assume Snomax has a buoyant density of approximately 1 – 1.2 g cm^{-3} based on the density of bacterial cells. As a result, Snomax should not pass through the density gradient medium during density gradient centrifugation experiments. If organic INSs with higher buoyant densities than 1.320 g cm^{-3} were centrifuged with OptiPrep™ these INSs would pass through the density gradient medium. In that case, a density gradient medium with a higher density should be used to separate the inorganic and organic INSs. However, a density gradient medium with a higher density was not needed in the current experiments.

2.2. Washing step using differential centrifugation

After density gradient centrifugation, a differential centrifugation washing step was used to remove any remaining density gradient medium from the high-density and low-density isolates (Figure 1, steps 5 – 7). Differential centrifugation is a common technique for separating particles in aqueous solutions based on sedimentation velocity. The high-density or low-density material resuspended in ultrapure water is centrifuged for a prescribed amount of time, and the materials with sufficiently high sedimentation velocities in water at the given centrifugal force will sediment to form a pellet at the bottom of the centrifugation tube, while the rest of the material remains suspended in the water. Unlike density gradient centrifugation, differential centrifugation does not involve the addition of any density gradient media, and only involves sedimentation through the solvent (water). Here, samples were centrifuged (Beckman Coulter Microfuge 20) for 10 minutes at 10,000 × g (Figure 1, step 5). Calculations illustrate that this centrifugation force and time is sufficient for organic particles with sizes greater than ~0.3 μm and inorganic particles with sizes greater than ~0.08 μm to pass through the water and sediment at the bottom of the tube (See SI, Section S2, Table S3). After centrifugation, the water and any material that did not pellet at the bottom of the tube (i.e. supernatant) was discarded, except the bottom ~5 μL which should contain the low- and high-density INSs in the form of pellets. The remaining material was resuspended in 750 μL of ultrapure water. Because

the final volume was approximately equal to the initial volume of the INS suspension that was centrifuged, the concentration of INSs in each isolate should be approximately equal to that of the low- or high-density INSs in the unprocessed sample if no material is lost.

2.3. Droplet-freezing experiments

A droplet freezing technique similar to Whale et al. (2015) was used to determine the freezing temperature spectrum of aqueous suspensions. We have previously used this technique to study the ice-nucleating properties of inorganic, organic, and environmental INS samples (Irish et al. 2019; Worthy et al. 2021; Xi et al. 2021; Yun et al. 2020; Yun et al. 2022). Hydrophobic glass slides (Hampton Research HR3-239) were rinsed with ultrapure water, dried with nitrogen gas, and placed on a cold stage (Grant Asymptote EF600 cryocooler). A micropipette was used to place twenty 1 μL drops of sample onto each slide (Figure S1). A second 1 μL drop of 0.01 M KNO_3 solution was then added to each sample droplet, bringing the total volume of each droplet to 2 μL, and the overall concentration of KNO_3 in each droplet to 0.005 M. The 0.01 M KNO_3 solution was prepared using ultrapure water. KNO_3 was added to combat the effects of any loss of K^+ ions during the density gradient centrifugation on the freezing properties of K-feldspar (Yun et al. 2020). KNO_3 was added to all samples for consistency. One slide of 20 droplets was prepared for each sample. A chamber with a digital camera was placed over the cold stage to isolate the droplets from the ambient air. A small flow of N_2 gas was passed through the chamber to prevent condensation during cooling. The cold stage temperature was decreased at a rate of 3 °C min^{-1} until all sample droplets were frozen while the digital camera attached to the chamber recorded video of the freezing process. The freezing temperature of each droplet was determined by processing the recorded video and cold stage temperature data via a MATLAB script (Worthy et al. 2021; Xi et al. 2021). The cold stage temperature measurements had an uncertainty of approximately ± 0.25 °C according to the manufacturer specifications. This uncertainty was verified by measuring the melting points of water and dodecane and comparing the measured values with literature values (Lide 2001). Because KNO_3 was added to all droplets, all freezing

temperatures reported here were corrected for the freezing point depression (0.0186 °C) caused by the solute. For details see SI Section S3.

The concentration of ice nucleating substances per liter of solution $[INS(T)]$ (L^{-1}) was calculated for each sample using the following equation (Vali 1971):

$$[INS(T)] = \frac{-\ln(N_u(T)/N_0) \times 2}{V} \quad (1)$$

Where $N_u(T)$ is the number of droplets in an experiment that are unfrozen at temperature T, N_0 is the total number of droplets in an experiment, and V is the volume of an individual droplet. The factor of 2 was included because the 1 µL drops of the INS suspensions were each diluted with an additional 1µL of KNO_3.

2.4. INS suspensions

The inorganic INS K-feldspar and the organic INS Snomax were used as test materials to evaluate this density gradient centrifugation method. Potassium-rich feldspar (K-feldspar) is an important component of atmospheric mineral dust and an effective ice nucleus (Atkinson et al. 2013; Harrison et al. 2016; Peckhaus et al. 2016; Whale et al. 2018; Yun et al. 2020). The density of K-feldspar is in the range of 2.55 – 2.63 g cm^{-3}, based on heavy liquid density separation (Haldar and Tišljar 2014; Wintle 1997; Woor et al. 2022). A K-feldspar sample was obtained from the Pacific Museum of Earth, University of British Columbia. The K-feldspar was ground into a powder using a mortar and pestle. The mineralogy of the resulting powder was 85% microcline ($KAlSi_3O_8$) and 15% albite ($NaAlSi_3O_8$) as determined by X-ray diffraction measurements. The particle sizes were around 3 µm based on the specific surface area of the particles in the powder determined with the Brunauer-Emmett-Teller nitrogen adsorption method (Yun et al. 2020). A 0.1 wt% suspension of this powder was prepared in ultrapure water and stirred overnight before experiments to ensure even particle distribution.

https://doi.org/10.26434/chemrxiv-2024-x8t26-v2 **ORCID:** https://orcid.org/0000-0002-5621-2323 Content not peer-reviewed by ChemRxiv. **License:** CC BY 4.0

Snomax is a commercial snow inducer composed of freeze-dried *P. syringae* cells and cell fragments. Bacterial cells, such as *P. syringae*, have densities in the range of 1.0 – 1.2 g /cm^3 (Bakken and Olsen 1983; Bratbak and Dundas 1984; Inoue et al. 2007; Neurohr, Amon, and Koch 2020), and we assume that Snomax has a similar density. The particulate matter in Snomax is primarily between 600 and 2000 nm in diameter (Wex et al. 2015). Snomax has been used previously to evaluate experimental methods for evaluating ice nuclei and as a proxy for atmospheric biological INS (Koop and Zobrist 2009; Wex et al. 2015; Whale et al. 2015; Worthy et al. 2021). A 1×10^{-4} wt% suspension of Snomax (Johnson Controls Snow) was prepared in ultrapure water and stored at 4 °C.

3. Results and discussion

3.1. Does the density gradient centrifugation technique introduce INSs?

Before testing our proposed density gradient centrifugation technique on INS suspensions, we tested the density gradient centrifugation technique using ultrapure water to establish if the technique introduces INS into the low- or high-density isolates. In these experiments, the high-density isolates overlap with the ultrapure water controls, indicating that the density gradient centrifugation technique was not introducing significant amounts of INS into the high-density isolates (Figure 2). The freezing curves of the low-density isolates overlap with the ultrapure water controls at temperatures less than approximately -23 °C (Figure 2). At warmer temperatures, the INS concentrations in the low-density isolates were significantly higher than in the ultrapure water controls in two of the three experiments. This suggests that some INSs were being introduced into the low-density isolates at some point in some experiments. INSs could be introduced from the lab air, the density gradient medium, materials used during density gradient centrifugation such as centrifuge tubes or pipette tips, and materials used in droplet freezing assays such as hydrophobic glass slides. Ultimately, the concentrations of INSs introduced are small and did not limit us from additional tests of the density gradient centrifugation technique.

Figure 2

3.2. Do trace amounts of the density gradient medium impact the freezing properties of the INSs?

Although our technique includes a washing step to remove the density gradient medium (OptiPrep™), some of the OptiPrep™ could still remain adsorbed to the INSs and influence their ice nucleation ability. To determine if this may be important in our experiments, we measured the ice nucleation ability of both INSs used in our experiments (K-feldspar and Snomax) in the presence of 1% OptiPrep™. This concentration is most likely an upper limit to the concentrations expected after the washing step in our experiments based on the amount of dilution in the washing steps. Corrections were made for the freezing point depression caused by OptiPrep™ using Eq. S2. For a concentration of 1% v/v the calculated freezing point depression was small (0.0036 °C).

In these experiments, the freezing curves of K-feldspar with 1% v/v OptiPrep™ overlap with those of K-feldspar without OptiPrep™, indicating that OptiPrep™ does not have a significant impact on the freezing properties of K-feldspar (Figure 3). The freezing curves for Snomax with 1% v/v OptiPrep™ also appear to overlap with those of Snomax without OptiPrep™, but on average, appear to be shifted slightly to warmer temperatures, suggesting that OptiPrep™ may slightly enhance the ice nucleation efficiency of Snomax.

Figure 3

To quantify if the INS concentrations were higher in the presence of 1% v/v OptiPrep™, we calculated the percentage of ice nucleation activity from the unprocessed suspension that was "recovered" after the addition of 1% v/v OptiPrep™ using the following equation:

$$\%\, recovery\ (T) = \frac{[INS(T)]_{OptiPrep}}{[INS(T)]_{unprocessed}} \times 100 \quad (2)$$

Where $[INS(T)]_{OptiPrep}$ is the concentration of INSs in the INS suspension with 1% v/v OptiPrep™ at temperature T and $[INS(T)]_{unprocessed}$ is the concentration of INSs in the corresponding unprocessed INS

https://doi.org/10.26434/chemrxiv-2024-x8t26-v2 **ORCID:** https://orcid.org/0000-0002-5621-2323

suspension without OptiPrep™ at temperature *T*. The number of INS particles should not change in these experiments, so this metric does not represent the recovery of physical INSs in this scenario.

For K-feldspar, the average recovery of ice nucleation activity in suspensions with 1% v/v OptiPrep™ added was 94% (median = 87%, 25^{th} – 75^{th} percentile = 51% to 116%) (Figure S2), further suggesting that the freezing properties of K-feldspar were not impacted by the addition of 1% v/v OptiPrep™. For Snomax, the average recovery of ice nucleation activity in suspensions with OptiPrep™ was 409% (median = 294%, 25^{th} – 75^{th} percentile = 206% to 520%). The recoveries suggest that the OptiPrep™ enhances the ice nucleation efficiency of Snomax by a factor of approximately 2 to 5 (Figure S2). However, this increase in INS concentration corresponds to just a 0.3 °C difference in median freezing temperatures between Snomax suspensions with and without OptiPrep™, which is close to the uncertainty of our cold stage measurements (±0.25 °C). In addition, the 1% v/v is an upper limit to the OptiPrep™ concentrations likely to be present in the experimental isolates. As such, the observed enhancement of ice nucleation by Snomax in the presence of 1% v/v OptiPrep™ is an upper limit to the effect of OptiPrep™ on Snomax ice nucleation in our experiments.

3.3. Are INSs lost during the washing step?

Before evaluating the ability of our density gradient centrifugation method to isolate organic and inorganic INSs, we investigated the differential centrifugation washing step alone (Figure 1, steps 5-7) to determine if both the organic and inorganic INSs are effectively recovered during the washing process. The recoveries from the washing step should serve as upper limits to the recoveries expected during density gradient centrifugation. The INS concentrations in the supernatants, which are discarded during the density gradient centrifugation protocol, were measured in addition to those in the pellet in order to discern if any INSs remain in the supernatant.

Before discussing the results for the washing step, we first discuss the variability of the INS concentrations for unprocessed K-feldspar and Snomax samples. The INS concentrations for K-feldspar, even for the unprocessed samples, fluctuate by up to a factor of 20 from experiment to experiment (Figure 4 and Figure S3). This variability is observed between replicates of the same K-feldspar solution performed on different days and between replicates of the same K-feldspar solution performed on the same day. This corresponds to median freezing temperature fluctuations of up to ~2.5 °C. This variability is likely due, at least in part, to inhomogeneity in the K-feldspar suspensions, rather than the uncertainty in our temperature measurements, which is small (±0.25 °C). INS concentrations for unprocessed Snomax samples also fluctuate by up to a factor of 20 from experiment to experiment (Figure 4 and Figure S3). This corresponds to median freezing temperature fluctuations of up to ~0.75 °C. This variability is also likely due, at least in part, to inhomogeneity in Snomax suspensions, but may also be influenced by the uncertainty in our temperature measurements (±0.25 °C). The variability for the unprocessed samples is important to keep in mind when analyzing the data below.

Figure 4

Next, we discuss the results for the washing step (Figure 4). The freezing curves for the resuspended pellets for both K-feldspar and Snomax overlap with the freezing curves for the unprocessed INS suspensions. This indicates that a large fraction of both K-feldspar and Snomax INSs are being recovered in the washing step. The K-feldspar supernatant contained significantly higher INS concentrations than the ultrapure water control, but significantly lower INS concentrations than the K-feldspar pellet. On average, the K-feldspar supernatant INS concentrations were ~15% of those of unprocessed K-feldspar. The Snomax supernatant also contained significantly higher INS concentrations than ultrapure water, but only slightly lower INS concentrations than the Snomax pellet. On average, the Snomax supernatant INS concentrations were ~30% of those of unprocessed Snomax. Losses of INSs to the supernatant may occur if the centrifugal pellet is disturbed during pipetting causing INSs to re-enter the supernatant. In addition, losses of INSs to the supernatant may occur if there are K-feldspar and Snomax particles in our suspensions that are too small to

sediment effectively during the differential centrifugation process. Our calculations suggest that the centrifugal force and time used during the washing step are sufficient for organic particles with sizes greater than ~0.3 μm and inorganic particles with sizes greater than ~0.08 μm to sediment (See SI, Section S2, Table S2). Therefore, if there are K-feldspar and Snomax particles present smaller than 0.08 μm and 0.3 μm, respectively, they may remain in the supernatant.

Percent recovery values were calculated using the following equation:

$$\%\, recovery\ (T) = \frac{[INS(T)]_{pellet}}{[INS(T)]_{unprocessed}} \times 100 \quad (3)$$

Where $[INS(T)]_{pellet}$ is the concentration of INSs in the resuspended pellet at temperature T and $[INS(T)]_{unprocessed}$ is the concentration of INSs in the corresponding unprocessed INS suspension without OptiPrep™ at temperature T.

For K-feldspar, the average % recovery in the centrifugal wash pellet was 159% (median = 100%, 25th – 75th percentile = 64% to 176%), indicating that the majority of the K-feldspar in the original suspension is successfully collected after washing (Figure 5 and Figure S4). The % recovery values varied significantly from experiment to experiment (see different symbol types in Figure S4). This variability can be explained, at least in part, by inhomogeneity in the K-feldspar suspensions, which leads to variability from experiment to experiment, even for unprocessed samples (see discussion above). In addition, the variability may be partially explained by small variability in pipetting technique from experiment to experiment. Variability in the pipetting technique could impact INS recovery by causing variability in how much of the centrifugal pellet is disturbed and reenters the supernatant during supernatant collection.

For Snomax, the average % recovery in the centrifugal wash pellet was 98% (median = 85%, 25th – 75th percentile = 56% to 120%), indicating that the majority of the Snomax in the original suspension is successfully collected after washing (Figure 5 and Figure S4). Much like K-feldspar, the Snomax %

recovery varies significantly from experiment to experiment (see different symbol types in Figure S4). This variability can also likely be explained, at least in part, by inhomogeneity in the Snomax suspensions. In addition, slight variability in pipetting technique from experiment to experiment could also explain the variability in the % recovery. Nevertheless, the majority of K-feldspar and Snomax INSs are recovered in the pellet after washing via differential centrifugation.

Figure 5

3.4. Do all the K-feldspar INSs get recovered in the high-density isolate?

In order to determine the recovery of inorganic INSs in the high-density isolate and if inorganic INSs contaminate the low-density isolate, tests were conducted with K-feldspar (density = 2.44 – 2.63 g cm^{-3}), an effective inorganic INS (Figure 6). For this case, the freezing curves for the high-density isolates partially overlapped with the unprocessed samples, but on average were shifted to slightly colder (~1 °C) temperatures indicating that most of the K-feldspar INSs were captured in the high-density isolate, but not all. The freezing curves for the low-density isolates overlapped with the ultrapure water control, indicating that the K-feldspar INSs were not contaminating the low-density isolates.

Figure 6

For the K-feldspar data, percent recovery values were calculated using Eq. 3 with the concentration of INSs in the high-density isolate in place of the concentration of INSs in the wash pellet. K-feldspar INSs were present in the high-density isolate with an average recovery of 54% (median = 49%, 25^{th} – 75^{th} percentile = 15% - 87%) (Figure 5 and Figure S5). The recoveries varied significantly between experimental replicates (see different symbol types in Figure S5). This variability can be explained, at least in part, by inhomogeneity in the K-feldspar suspensions, which leads to variability from experiment to experiment (see discussion above).

The % recovery values less than 100 % for K-feldspar INSs may be due to loss of K-feldspar to the vessel walls during density gradient centrifugation. In addition, some of the K-feldspar INSs may have been discarded with the density gradient medium if they were small in size and therefore not able to sediment completely (See SI, Section 1, Table S1). K-feldspar loss could also occur if the pellet is disturbed when removing the density gradient medium, leading to K-feldspar INSs reentering the density gradient medium and being discarded.

Overall, the results of density gradient centrifugation performed on a K-feldspar suspension are consistent with a large fraction of the K-feldspar INSs being isolated in the high-density isolate with minimal contamination of the low-density isolate.

3.5. Do all the Snomax INSs get recovered in the low-density isolate?

In order to determine the recovery of organic INSs in the low-density isolate and if organic INSs contaminate the high-density isolate using our proposed density gradient centrifugation method, tests were conducted with Snomax (estimated density = 1.0 – 1.2 g cm^{-3}), a highly effective organic INS (Figure 7). The freezing curves for the low-density isolates were similar to the unprocessed samples, but shifted to slightly colder (~1 °C) temperatures, indicating that a large fraction of the Snomax INSs were recovered in the low-density isolate, but not all. For the high-density isolates, one of the freezing curves overlaps with the ultrapure water blanks, but two of the freezing curves were shifted to warmer temperatures at low INS concentrations. This suggests that the high-density isolate was contaminated by a relatively small concentration of Snomax in some, but not all, experimental replicates.

Figure 7

In all cases, the concentrations of Snomax in the high-density isolates were less than 1% of those in the unprocessed Snomax suspensions. The fact that contamination did not occur in all replicates suggests that this contamination can be reduced or eliminated through careful experimental technique. If not all low-

density INSs are successfully collected when pipetting off the low-density material, some low-density INSs may come into contact with micropipette tips used to collect the high-density material thereby contaminating the high-density isolate.

Percent recovery values were calculated using Eq. 3 with the concentration of INSs in the low-density isolate in place of the concentration of INSs in the wash pellet. Snomax INSs were present in the low-density isolate with an average recovery of 27% (median = 23%, 25^{th} – 75^{th} percentile = 17% - 34%) (Figure 5 and Figure S6). There was variability in recovery from experiment to experiment (see different symbol types in Figure S6), which can likely be explained, at least in part, by inhomogeneity in the Snomax solutions, which leads to variability from experiment to experiment, even within unprocessed suspensions.

The % recovery value less than 100 % for Snomax INSs may be explained by Snomax INSs sticking to vessel walls or incomplete collection of the low-density fraction during pipetting. Snomax INSs will be concentrated at the interface between the water layer and the density gradient medium after centrifugation. Improper pipetting may lead to incomplete collection of the Snomax INSs. Pipetting can also lead to mechanical mixing at the interface and some loss of the Snomax INSs into the density gradient medium.

3.6. For mixtures, what percentage of K-feldspar and Snomax INSs are recovered in the high-density and low-density isolates, respectively?

We evaluated the recoveries of inorganic and organic INSs in the high- and low-density isolates, respectively, using a mixture of K-feldspar and Snomax INSs. This mixture was prepared by combining the previously described K-feldspar and Snomax solutions in a 1:1 ratio. The freezing results for the mixture were compared to unprocessed K-feldspar and Snomax suspensions, which were prepared by combining the original K-feldspar and Snomax INS suspensions with ultrapure water in a 1:1 ratio (Figure 8). The freezing curves for the high-density isolates were similar to those for unprocessed K-feldspar, but shifted to slightly colder (~1 °C) temperatures, suggesting that a large fraction of the K-feldspar INSs, but not all,

were recovered in the high-density isolate. The freezing curves for the low-density isolates were similar to those for unprocessed Snomax, but also shifted to slightly colder (~0.75 °C) temperatures, suggesting that a large fraction of Snomax INSs, but not all, were recovered in the low-density isolate.

Figure 8

To determine recoveries, the INS concentrations in the high- and low-density isolates were compared to unprocessed individual suspensions of K-feldspar and Snomax, respectively. K-feldspar INSs were present in the high-density isolate with an average recovery of 56% (median = 49%, 25^{th} – 75^{th} percentile = 37% - 65%) (Figure 5 and Figure S7). The % recovery of K-feldspar INS was similar to the % recovery of K-feldspar INS in a suspension of just K-feldspar (Figure 5), suggesting that this density gradient centrifugation technique is able to recover inorganic INSs in a mixture with a comparable efficiency to inorganic INSs in a lone suspension.

Snomax INSs were present in the low-density isolate with an average recovery of 25% (median = 22%, 25^{th} – 75^{th} percentile = 18% - 37%) (Figure 5 and Figure S7). The average % recovery of Snomax INS in the mixture was equal to that of Snomax INS from a suspension of just Snomax (Figure 5), suggesting that this density gradient centrifugation technique is able to recover organic INSs in a mixture with a comparable efficiency to organic INSs in a lone suspension.

4. Conclusions

In this work we presented a method for separating and quantifying organic and inorganic INSs via density gradient centrifugation combined with a droplet freezing technique. This method takes advantage of the significant difference between the densities of organic INSs ($\lesssim 1.6$ g cm^{-3}) and inorganic INSs ($\gtrsim 2.1$ g cm^{-3}). We characterized the performance of this method using K-rich feldspar and Snomax as test inorganic and organic INSs, respectively. The main results from these studies are summarized in Figure 5. The

https://doi.org/10.26434/chemrxiv-2024-x8t26-v2 **ORCID:** https://orcid.org/0000-0002-5621-2323

recovery of K-feldspar in the high-density isolate after density gradient centrifugation was on average 54%, suggesting that many K-feldspar INSs, but not all, were successfully recovered. There was no evidence of cross contamination of K-feldspar INSs in the low-density isolate. Similarly, the recovery of Snomax in the low-density isolate was on average 27%, suggesting that many Snomax INSs, but not all, were successfully recovered. In contrast, there was evidence of contamination of the high-density isolate with a small concentration of Snomax INSs in two out of three experimental replicates. A mixture of K-feldspar and Snomax was successfully separated, with recoveries of K-feldspar INSs in the high-density isolate and Snomax INSs in the low-density isolate comparable to those observed for K-feldspar and Snomax individually.

Recoveries less than 100% can most likely be explained by losses of INSs to vessel walls, accidental mixing of the different density layers during pipetting, and incomplete collection of the high- and low-density material during pipetting. Contamination of the high-density isolate by small amounts of Snomax INSs can also likely be explained by incomplete collection of the low-density material, as this uncollected material left in the centrifuge tubes can easily contaminate the high-density isolate. This highlights pipetting technique and material collection as an area where improvements to the protocol would be beneficial. Specialty devices, instruments, and protocols have been developed for layering and material collection in density gradient centrifugation procedures (de Jonge 1979; Lawrence and Steward 2010; Work and Work 1978), which may help improve INS contamination and recoveries if integrated into our density gradient centrifugation procedure. Nevertheless, recovery values less than 100% are acceptable as long as they are quantified. The uncertainties associated with the concentrations of organic and inorganic INSs in the atmosphere can be several orders of magnitude, or more (Burrows et al. 2022; Kanji et al. 2017); hence, recoveries on the order of 30% or greater are acceptable, especially if they are known and can be accounted for. Overall, our results suggest that this technique shows promise for separating, quantifying, and characterizing inorganic and organic INSs. Additional studies are needed to determine if other types of inorganic and organic INSs have similar recoveries to K-feldspar and Snomax, respectively. Before this

technique can be applied to atmospheric samples of unknown composition, we need to establish an understanding of how this technique responds to a range of different INS types, sizes, and concentrations.

Acknowledgments

The authors thank Elena Polishchuk and Jessie Chen for their assistance with developing and executing the centrifugation protocols.

Funding

We acknowledge the support of the Natural Sciences and Engineering Research Council of Canada (NSERC), [funding reference number RGPIN-2023-05333].

ORCID

Will be added in list form by the typesetter if provided (not required).

References

Anderson, N. G., W. W. Harris, A. A. Barber, C. T. Rankin, and E. L. Candler. 1966. Separation of Subcellular Components and Viruses by Combined Rate- and Isopycnic-Zonal Centrifugation. *National Cancer Institute Monograph* 21:253–283.

Ansmann, A., M. Tesche, P. Seifert, D. Althausen, R. Engelmann, J. Fruntke, U. Wandinger, I. Mattis, and D. Müller. 2009. Evolution of the Ice Phase in Tropical Altocumulus: SAMUM Lidar Observations over Cape Verde. *Journal of Geophysical Research* 114 (D17208). doi:10.1029/2008JD011659.

Anthony, J. W., R. A. Bideaux, K. W. Bladh, and M. C. Nichols. 2001. Graphite. In *Handbook of Mineralogy*. Vol. Volume 1. Chantilly, VA: Mineralogical Society of America.

Atkinson, J. D., B. J. Murray, M. T. Woodhouse, T. F. Whale, K. J. Baustian, K. S. Carslaw, S. Dobbie, D. O'Sullivan, and T. L. Malkin. 2013. The Importance of Feldspar for Ice Nucleation by Mineral Dust in Mixed-Phase Clouds. *Nature* 498 (7454):355–358. doi:10.1038/nature12278.

Backman, A., and J. K. Jansson. 2004. Degradation of 4-Chlorophenol at Low Temperature and during Extreme Temperature Fluctuations by Arthrobacter Chlorophenolicus A6. *Microbial Ecology* 48:246–253. doi:10.1007/s00248-003-2026-3.

Bagheri, G., and C. Bonadonna. 2016. Aerodynamics of Volcanic Particles: Characterization of Size, Shape, and Settling Velocity. In *Volcanic Ash: Hazard Observation*, ed. S. Mackie, K. Cashman, H. Ricketts, A. Rust, and M. Watson, 39–52. Elsevier. doi:10.1016/B978-0-08-100405-0.00005-7.

Bakken, L. R. 1985. Separation and Purification of Bacteria from Soil. *Applied and Environmental Microbiology*, 1482–1487. doi:10.1128/aem.49.6.1482-1487.1985.

Bakken, L. R., and R. A. Olsen. 1983. Buoyant Densities and Dry-Matter Contents of Microorganisms: Conversion of a Measured Biovolume into Biomass. *Applied and Environmental Microbiology* 45 (4):1188–1195. doi:10.1128/aem.45.4.1188-1195.1983.

Boucher, O., D. Randall, P. Artaxo, C. Bretherton, G. Feingold, P. Forster, V.-M. Kerminen, Y. Kondo, H. Liao, U. Lohmann, et al. 2013. Clouds and Aerosols. *Climate Change 2013 the Physical Science Basis: Working Group I Contribution to the Fifth Assessment Report of the Intergovernmental Panel on Climate Change*. 571–658. doi:10.1017/CBO9781107415324.016.

Bratbak, G., and I. Dundas. 1984. Bacterial Dry Matter Content and Biomass Estimations. *Applied and Environmental Microbiology* 48 (4):755–757. doi:10.1128/aem.48.4.755-757.1984.

Burrows, S. M., C. S. McCluskey, G. Cornwell, I. Steinke, K. Zhang, B. Zhao, M. Zawadowicz, A. Raman, G. Kulkarni, S. China, et al. 2022. Ice-Nucleating Particles That Impact Clouds and Climate: Observational and Modeling Research Needs. *Reviews of Geophysics* 60 (2). doi:10.1029/2021RG000745.

Christner, B. C., R. Cai, C. E. Morris, K. S. McCarter, C. M. Foreman, M. L. Skidmore, S. N. Montross, and D. C. Sands. 2008. Geographic, Seasonal, and Precipitation Chemistry Influence on the

Abundance and Activity of Biological Ice Nucleators in Rain and Snow. *Proceedings of the National Academy of Sciences* 105 (48):18854–18859. doi:10.1073/pnas.0809816105.

Conen, F., C. E. Morris, J. Leifeld, M. V. Yakutin, and C. Alewell. 2011. Biological Residues Define the Ice Nucleation Properties of Soil Dust. *Atmospheric Chemistry and Physics* 11 (18):9643–9648. doi:10.5194/ACP-11-9643-2011.

Corbin, J. C., P. J. G. Rehbein, G. J. Evans, and J. P. D. Abbatt. 2012. Combustion Particles as Ice Nuclei in an Urban Environment: Evidence from Single-Particle Mass Spectrometry. *Atmospheric Environment* 51:286–292. doi:10.1016/j.atmosnev.2012.01.007.

Cziczo, D. J., D. M. Murphy, P. K. Hudson, and D. S. Thomson. 2004. Single Particle Measurements of the Chemical Composition of Cirrus Ice Residue during CRYSTAL-FACE. *Journal of Geophysical Research: Atmospheres* 109 (D04201). doi:10.1029/2003JD004032.

Daily, M. I., M. D. Tarn, T. F. Whale, and B. J. Murray. 2022. An Evaluation of the Heat Test for the Ice-Nucleating Ability of Minerals and Biological Material. *Atmospheric Measurement Techniques* 15:2635–2665. doi:10.5194/amt-15-2635-2022.

David, R. O., C. Marcolli, J. Fahrni, Y. Qiu, Y. A. Perez Sirkin, V. Molinero, F. Mahrt, D. Brühwiler, U. Lohmann, and Z. A. Kanji. 2019. Pore Condensation and Freezing Is Responsible for Ice Formation below Water Saturation for Porous Particles. *Proceedings of the National Academy of Sciences* 116 (17):8184–8189. doi:10.1073/pnas.1813647116.

de Jonge, V. N. 1979. Quantitative Separation of Benthic Diatoms from Sediments Using Density Gradient Centrifugation in the Colloidal Silica Ludox-TM. *Marine Biology* 51 (3):267–278. doi:10.1007/BF00386807/METRICS.

DeMott, P. J., K. Sassen, M. R. Poellot, D. Baumgardner, D. C. Rogers, S. D. Brooks, A. J. Prenni, and S. M. Kreidenweis. 2003. African Dust Aerosols as Atmospheric Ice Nuclei. *Geophysical Research Letters* 30 (14). doi:10.1029/2003GL017410.

Dinar, E., T. F. Mentel, and Y. Rudich. 2006. The Density of Humic Acids and Humic like Substances (HULIS) from Fresh and Aged Wood Burning and Pollution Aerosol Particles. *Atmospheric Chemistry and Physics* 6:5213–5224. doi:10.5194/acp-6-5213-2006.

Dreischmeier, K., C. Budke, L. Wiehemeier, T. Kottke, and T. Koop. 2017. Boreal Pollen Contain Ice-Nucleating as Well as Ice-Binding "antifreeze" Polysaccharides. *Scientific Reports* 7 (1):1–13. doi:10.1038/srep41890.

Durham, O. C. 1943. The Volumetric Incidence of Atmospheric Allergens. *Journal of Allergy* 14 (6):445–461.

Haldar, S. K., and J. Tišljar. 2014. Basic Mineralogy. In *Introduction to Mineralogy and Petrology*, 39–79. doi:10.1016/B978-0-12-408133-8.00002-X.

Harding, S. E. 1992. Sedimentation Analysis of Polysaccharides. In *Analytical Ultracentrifugation in Biochemistry and Polymer Science*, 495–516.

Harrington, J. B., and K. Metzger. 1963. Ragweed Pollen Density. *American Journal of Botany* 50 (6):532–539. doi:10.2307/2440028.

Harrison, A. D., T. F. Whale, M. A. Carpenter, M. A. Holden, L. Neve, D. O'Sullivan, J. Vergara Temprado, and B. J. Murray. 2016. Not All Feldspars Are Equal: A Survey of Ice Nucleating Properties across the Feldspar Group of Minerals. *Atmospheric Chemistry and Physics* 16:10927–10940. doi:10.5194/acp-16-10927-2016.

Hazardous Substances Data Bank (HSDB). 2023. Accessed December 12, 2023. https://pubchem.ncbi.nlm.nih.gov/source/Hazardous%20Substances%20Data%20Bank%20(HSDB).

Hill, T. C.J., P. J. Demott, Y. Tobo, J. Fröhlich-Nowoisky, B. F. Moffett, G. D. Franc, and S. M. Kreidenweis. 2016. Sources of Organic Ice Nucleating Particles in Soils. *Atmospheric Chemistry and Physics* 16 (11):7195–7211. doi:10.5194/ACP-16-7195-2016.

Hoose, C., and O. Möhler. 2012. Heterogeneous Ice Nucleation on Atmospheric Aerosols: A Review of Results from Laboratory Experiments. *Atmospheric Chemistry and Physics* 12 (20):9817–9854. doi:10.5194/acp-12-9817-2012.

Inoue, K., M. Nishimura, B. B. Nayak, and K. Kogure. 2007. Separation of Marine Bacteria According to Buoyant Density by Use of the Density-Dependent Cell Sorting Method. *Applied and Environmental Microbiology* 73 (4):1049–1053. doi:10.1128/AEM.01158-06.

Irish, V. E., S. J. Hanna, Y. Xi, M. Boyer, E. Polishchuk, M. Ahmed, J. Chen, J. P. D. Abbatt, M. Gosselin, R. Chang, et al. 2019. Revisiting Properties and Concentrations of Ice-Nucleating Particles in the Sea Surface Microlayer and Bulk Seawater in the Canadian Arctic during Summer. *Atmospheric Chemistry and Physics* 19 (11):7775–7787. doi:10.5194/acp-19-7775-2019.

Iwata, A., and A. Matsuki. 2018. Characterization of Individual Ice Residual Particles by the Single Droplet Freezing Method: A Case Study in the Asian Dust Outflow Region. *Atmospheric Chemistry and Physics* 18:1785–1804. doi:10.5194/acp-18-1785-2018.

Kanji, Z. A., L. A. Ladino, H. Wex, Y. Boose, M. Burkert-Kohn, D. J. Cziczo, and M. Krämer. 2017. Overview of Ice Nucleating Particles. *Meteorological Monographs* 58:1.1-1.33. doi:10.1175/AMSMONOGRAPHS-D-16-0006.1.

Knopf, D. A., and P. A. Alpert. 2013. A Water Activity Based Model of Heterogeneous Ice Nucleation Kinetics for Freezing of Water and Aqueous Solution Droplets. *Faraday Discussions* 165:513–534. doi:10.1039/c3fd00035d.

Knopf, D. A., P. A. Alpert, and B. Wang. 2018. The Role of Organic Aerosol in Atmospheric Ice Nucleation: A Review. *ACS Earth and Space Chemistry* 2:168–202. doi:10.1021/acsearthspacechem.7b00120.

Knopf, D. A., J. C. Charnawskas, P. Wang, B. Wong, J. M. Tomlin, K. A. Jankowski, M. Fraund, D. P. Veghte, S. China, A. Laskin, et al. 2022. Micro-Spectroscopic and Freezing Characterization of Ice-Nucleating Particles Collected in the Marine Boundary Layer in the Eastern North Atlantic. *Atmospheric Chemistry and Physics* 22:5377–5398. doi:10.5194/acp-22-5377-2022.

Knopf, D. A., B. Wang, A. Laskin, R. C. Moffet, and M. K. Gilles. 2010. Heterogeneous Nucleation of Ice on Anthropogenic Organic Particles Collected in Mexico City. *Geophysical Research Letters* 37 (L11803). doi:10.1029/2010GL043362.

Koop, T., and B. J. Murray. 2016. A Physically Constrained Classical Description of the Homogeneous Nucleation of Ice in Water. *The Journal of Chemical Physics* 145 (211915). doi:10.1063/1.4962355.

Koop, T., and B. Zobrist. 2009. Parameterizations for Ice Nucleation in Biological and Atmospheric Systems. *Physical Chemistry Chemical Physics* 11 (46):10839–10850. doi:10.1039/b914289d.

Kumar, A., C. Marcolli, B. Luo, and T. Peter. 2018. Ice Nucleation Activity of Silicates and Aluminosilicates in Pure Water and Aqueous Solutions-Part 1: The K-Feldspar Microcline. *Atmospheric Chemistry and Physics* 18 (10):7057–7079. doi:10.5194/acp-18-7057-2018.

Kumar, A., C. Marcolli, and T. Peter. 2019a. Ice Nucleation Activity of Silicates and Aluminosilicates in Pure Water and Aqueous Solutions-Part 2: Quartz and Amorphous Silica. *Atmospheric Chemistry and Physics* 19 (9):6035–6058. doi:10.5194/acp-19-6035-2019.

Kumar, A., C. Marcolli, and T. Peter. 2019b. Ice Nucleation Activity of Silicates and Aluminosilicates in Pure Water and Aqueous Solutions-Part 3: Aluminosilicates. *Atmospheric Chemistry and Physics* 19 (9):6059–6084. doi:10.5194/acp-19-6059-2019.

Lammers, W. T. 1963. Density-Gradient Separation of Organic and Inorganic Particles by Centrifugation. *Science* 139 (3561):1298–1299.

Lawrence, J. E., and G. F. Steward. 2010. Purification of Viruses by Centrifugation. In *Manual of Aquatic and Viral Ecology*, ed. S. W. Wilhelm, M. G. Weinbauer, and C. A. Suttle, 166–181. ASLO. doi:10.4319/mave.2010.978-0-9845591-0-7.166.

Lide, R. D. 2001. *CRC Handbook of Chemistry and Physics*. CRC Press Taylor and Francis Group.

Lindahl, V., and L. R. Bakken. 1995. Evaluation of Methods for Extraction of Bacteria from Soil. *FEMS Microbiology Ecology* 16:135–142. doi:10.1111/j.1574-6941.1995.tb00277.x.

Lohmann, U. 2002. A Glaciation Indirect Aerosol Effect Caused by Soot Aerosols. *Geophysical Research Letters* 29 (4):11-1 – 11-4. doi:10.1029/2001GL014357.

Lohmann, U., and J. Feichter. 2005. Global Indirect Aerosol Effects: A Review. *Atmospheric Chemistry and Physics* 5:715–737. doi:10.5194/acp-5-715-2005.

Murray, B. J., D. O'Sullivan, J. D. Atkinson, and M. E. Webb. 2012. Ice Nucleation by Particles Immersed in Supercooled Cloud Droplets. *Chemical Society Reviews* 41 (19):6519–6554. doi:10.1039/c2cs35200a.

National Center for Biotechnology Information. 2023. Periodic Table of Elements. Accessed December 12, 2023. https://pubchem.ncbi.nlm.nih.gov/periodic-table/.

Neurohr, G. E., A. Amon, and D. H. Koch. 2020. Relevance and Regulation of Cell Density. *Trends in Cell Biology* 30 (3):213–225. doi:10.1016/j.tcb.2019.12.006.

O'Sullivan, D., B. J. Murray, T. L. Malkin, T. F. Whale, N. S. Umo, J. D. Atkinson, H. C. Price, K. J. Baustian, J. Browse, and M. E. Webb. 2014. Ice Nucleation by Fertile Soil Dusts: Relative Importance of Mineral and Biogenic Components. *Atmospheric Chemistry and Physics* 14 (4):1853–1867. doi:10.5194/acp-14-1853-2014.

Peckhaus, A., A. Kiselev, T. Hiron, M. Ebert, and T. Leisner. 2016. A Comparative Study of K-Rich and Na/Ca-Rich Feldspar Ice-Nucleating Particles in a Nanoliter Droplet Freezing Assay. *Atmospheric Chemistry and Physics* 16 (18):11477–11496. doi:10.5194/acp-16-11477-2016.

Perkins, R. J., S. M. Gillette, T. C. J. Hill, and P. J. DeMott. 2020. The Labile Nature of Ice Nucleation by Arizona Test Dust. *ACS Earth and Space Chemistry* 4 (1):133–141. doi:10.1021/acsearthspacechem.9b00304.

Pratt, K. A., P. J. DeMott, J. R. French, Z. Wang, D. L. Westphal, A. J. Heymsfield, C. H. Twohy, A. J. Prenni, and K. A. Prather. 2009. In Situ Detection of Biological Particles in Cloud Ice-Crystals. *Nature Geoscience* 2 (6):398–401. doi:10.1038/ngeo521.

Prenni, A. J., P. J. Demott, D. C. Rogers, S. M. Kreidenweis, G. M. Mcfarquhar, G. Zhang, and M. R. Poellot. 2009. Ice Nuclei Characteristics from M-PACE and Their Relation to Ice Formation in Clouds. *Tellus, Series B: Chemical and Physical Meteorology* 61 B (2):436–448. doi:10.1111/j.1600-0889.2009.00415.x.

Pummer, B. G., C. Budke, S. Augustin-Bauditz, D. Niedermeier, L. Felgitsch, C. J. Kampf, R. G. Huber, K. R. Liedl, T. Loerting, T. Moschen, et al. 2015. Ice Nucleation by Water-Soluble Macromolecules. *Atmospheric Chemistry and Physics* 15 (8):4077–4091. doi:10.5194/acp-15-4077-2015.

Saxby, J., F. Beckett, K. Cashman, A. Rust, and E. Tennant. 2018. The Impact of Particle Shape on Fall Velocity: Implications for Volcanic Ash Dispersion Modelling. *Journal of Volcanology and Geothermal Research* 362:32–48. doi:10.1016/j.jvolgeores.2018.08.006.

Schneider, J., K. Höhler, P. Heikkilä, J. Keskinen, B. Bertozzi, P. Bogert, T. Schorr, N. Silas Umo, F. Vogel, Z. Brasseur, et al. 2021. The Seasonal Cycle of Ice-Nucleating Particles Linked to the Abundance of Biogenic Aerosol in Boreal Forests. *Atmospheric Chemistry and Physics* 21 (5):3899–3918. doi:10.5194/ACP-21-3899-2021.

Schnell, R. C., and G. Vali. 1975. Freezing Nuclei in Marine Waters. *Tellus A: Dynamic Meteorology and Oceanography* 27 (3):321. doi:10.3402/TELLUSA.V27I3.9911.

Schrod, J., E. S. Thomson, D. Weber, J. Kossmann, C. Pöhlker, J. Saturno, F. Ditas, P. Artaxo, V. Clouard, J. M. Saurel, et al. 2020. Long-Term Deposition and Condensation Ice-Nucleating Particle Measurements from Four Stations across the Globe. *Atmospheric Chemistry and Physics* 20 (24):15983–16006. doi:10.5194/ACP-20-15983-2020.

Tan, I., T. Storelvmo, and M. D. Zelinka. 2016. Observational Constraints on Mixed-Phase Clouds Imply Higher Climate Sensitivity. *Science* 352 (6282):224–227. doi: 10.1126/science.aad5300DF.

Vali, G. 1971. Quantitative Evaluation of Experimental Results on the Heterogeneous Freezing Nucleation of Supercooled Liquids. *Journal of the Atmospheric Sciences* 28 (3):402–409. doi:10.1175/1520-0469(1971)028<0402:QEOERA>2.0.CO;2.

Vali, G., P. J. Demott, O. Möhler, and T. F. Whale. 2015. Technical Note: A Proposal for Ice Nucleation Terminology. *Atmospheric Chemistry and Physics* 15 (18):10263–10270. doi:10.5194/acp-15-10263-2015.

van Hout, R., and J. Katz. 2004. A Method for Measuring the Density of Irregularly Shaped Biological Aerosols Such as Pollen. *Journal of Aerosol Science* 35 (11):1369–1384. doi:10.1016/j.jaerosci.2004.05.008.

Vogel, A., S. Diplas, A. J. Durant, A. S. Azar, M. F. Sunding, W. I. Rose, A. Sytchkova, C. Bonadonna, K. Krüger, and A. Stohl. 2017. Reference Data Set of Volcanic Ash Physicochemical and Optical Properties. *Journal of Geophysical Research: Atmospheres* 122 (17):9485–9514. doi:10.1002/2016JD026328.

Westbrook, C. D., and A. J. Illingworth. 2013. The Formation of Ice in a Long-Lived Supercooled Layer Cloud. *Quarterly Journal of the Royal Meteorological Society* 139:2209–2221. doi:10.1002/qj.2096.

Wex, H., S. Augustin-Bauditz, Y. Boose, C. Budke, J. Curtius, K. Diehl, A. Dreyer, F. Frank, S. Hartmann, N. Hiranuma, et al. 2015. Intercomparing Different Devices for the Investigation of Ice Nucleating Particles Using Snomax® as Test Substance. *Atmospheric Chemistry and Physics* 15 (3):1463–1485. doi:10.5194/acp-15-1463-2015.

Whale, T. F., M. A. Holden, T. W. Wilson, D. O'Sullivan, and B. J. Murray. 2018. The Enhancement and Suppression of Immersion Mode Heterogeneous Ice-Nucleation by Solutes. *Chemical Science* 9 (17):4142–4151. doi:10.1039/c7sc05421a.

Whale, T. F., B. J. Murray, D. O'Sullivan, T. W. Wilson, N. S. Umo, K. J. Baustian, J. D. Atkinson, D. A. Workneh, and G. J. Morris. 2015. A Technique for Quantifying Heterogeneous Ice Nucleation in Microlitre Supercooled Water Droplets. *Atmospheric Measurement Techniques* 8 (6):2437–2447. doi:10.5194/amt-8-2437-2015.

Wilson, T. W., L. A. Ladino, P. A. Alpert, M. N. Breckels, I. M. Brooks, J. Browse, S. M. Burrows, K. S. Carslaw, J. A. Huffman, C. Judd, et al. 2015. A Marine Biogenic Source of Atmospheric Ice-Nucleating Particles. *Nature* 525 (7568):234–238. doi:10.1038/nature14986.

Wintle, A. G. 1997. Luminescence Dating: Laboratory Procedures and Protocols. *Radiation Measurements* 27 (5–6):769–817.

Woor, S., J. A. Durcan, S. L. Burrough, A. Parton, and D. S. G. Thomas. 2022. Evaluating the Effectiveness of Heavy Liquid Density Separation in Isolating K-Feldspar Grains Using Alluvial Sediments from the Hajar Mountains, Oman. *Quaternary Geochronology* 72:101368. doi:10.1016/J.QUAGEO.2022.101368.

Work, T. S., and E. Work, eds. 1978. Centrifugation in Conventional Rotors. In *Laboratory Techniques in Biochemistry and Molecular Biology*, 6:97–119. Elsevier. doi:10.1016/S0075-7535(08)70158-X.

Worthy, S. E., A. Kumar, Y. Xi, J. Yun, J. Chen, C. Xu, V. E. Irish, P. Amato, and A. K. Bertram. 2021. The Effect of (NH4)2SO4 on the Freezing Properties of Non-Mineral Dust Ice-Nucleating Substances of Atmospheric Relevance. *Atmospheric Chemistry and Physics* 21:14631–14648. doi:10.5194/acp-21-14631-2021.

Xi, Y., A. Mercier, C. Kuang, J. Yun, A. Christy, L. Melo, M. T. Maldonado, J. A. Raymond, and A. K. Bertram. 2021. Concentrations and Properties of Ice Nucleating Substances in Exudates from Antarctic Sea-Ice Diatoms. *Environmental Science: Processes & Impacts* 23 (2):323–334. doi:10.1039/D0EM00398K.

Xi, Y., C. Xu, A. Downey, R. Stevens, J. O. Bachelder, J. King, P. L. Hayes, and A. K. Bertram. 2022. Ice Nucleating Properties of Airborne Dust from an Actively Retreating Glacier in Yukon, Canada. *Environmental Science: Atmospheres* 2 (4):714–726. doi:10.1039/D1EA00101A.

Yun, J., E. Evoy, S. E. Worthy, M. Fraser, D. Veber, A. Platt, K. Rawlings, S. Sharma, W. R. Leaitch, and A. Bertram. 2022. Ice Nucleating Particles in the Canadian High Arctic during the Fall of 2018. *Environmental Science: Atmospheres*. doi:10.1039/D1EA00068C.

Yun, J., N. Link, A. Kumar, A. Shchukarev, J. Davidson, A. Lam, C. Walters, Y. Xi, J.-F. Boily, and A. K. Bertram. 2020. Surface Composition Dependence on the Ice Nucleating Ability of Potassium-Rich Feldspar. *ACS Earth and Space Chemistry* 4 (6):873–881. doi:10.1021/acsearthspacechem.0c00077.

Figures

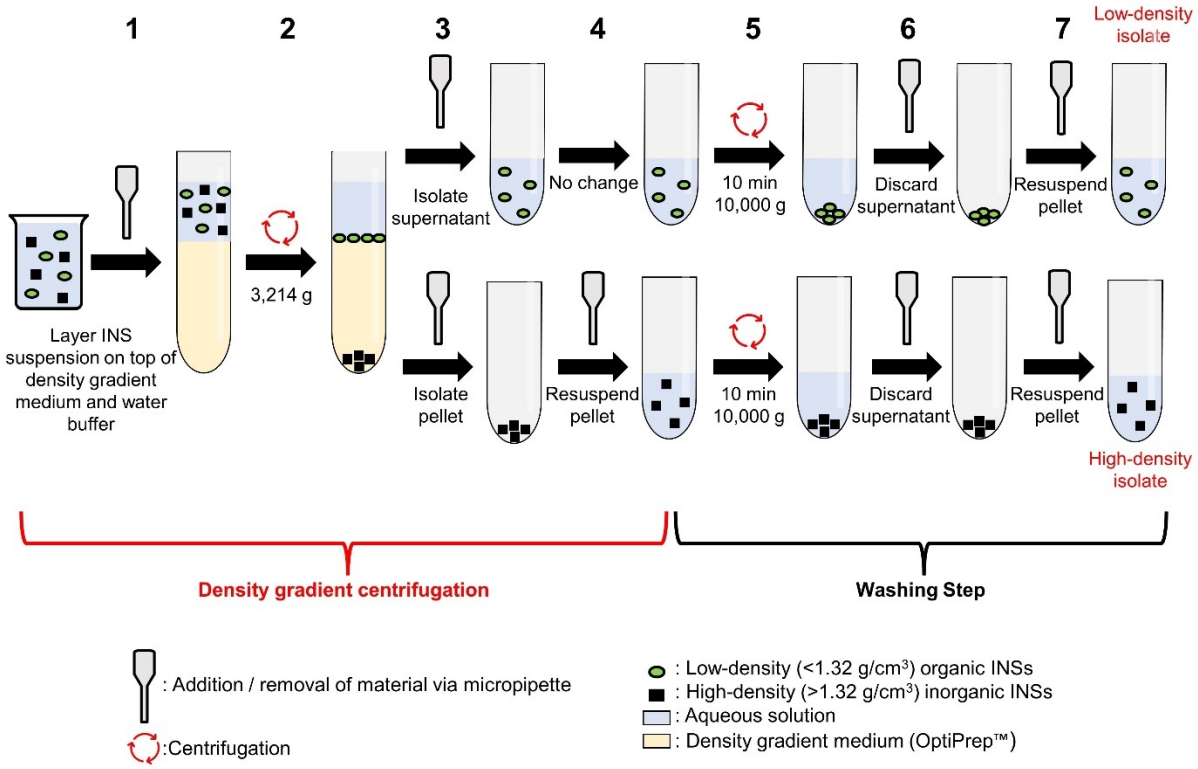

Figure 1. Schematic of the density gradient centrifugation procedure illustrating density gradient centrifugation (steps 1-2), isolation of the low-density material and high-density pellet (steps 3-4), and the washing step (steps 5-7) to remove excess water-soluble density gradient medium, resulting in the finalized low- and high-density isolates for droplet freezing experiments.

https://doi.org/10.26434/chemrxiv-2024-x8t26-v2 **ORCID:** https://orcid.org/0000-0002-5621-2323 Content not peer-reviewed by ChemRxiv. **License:** CC BY 4.0

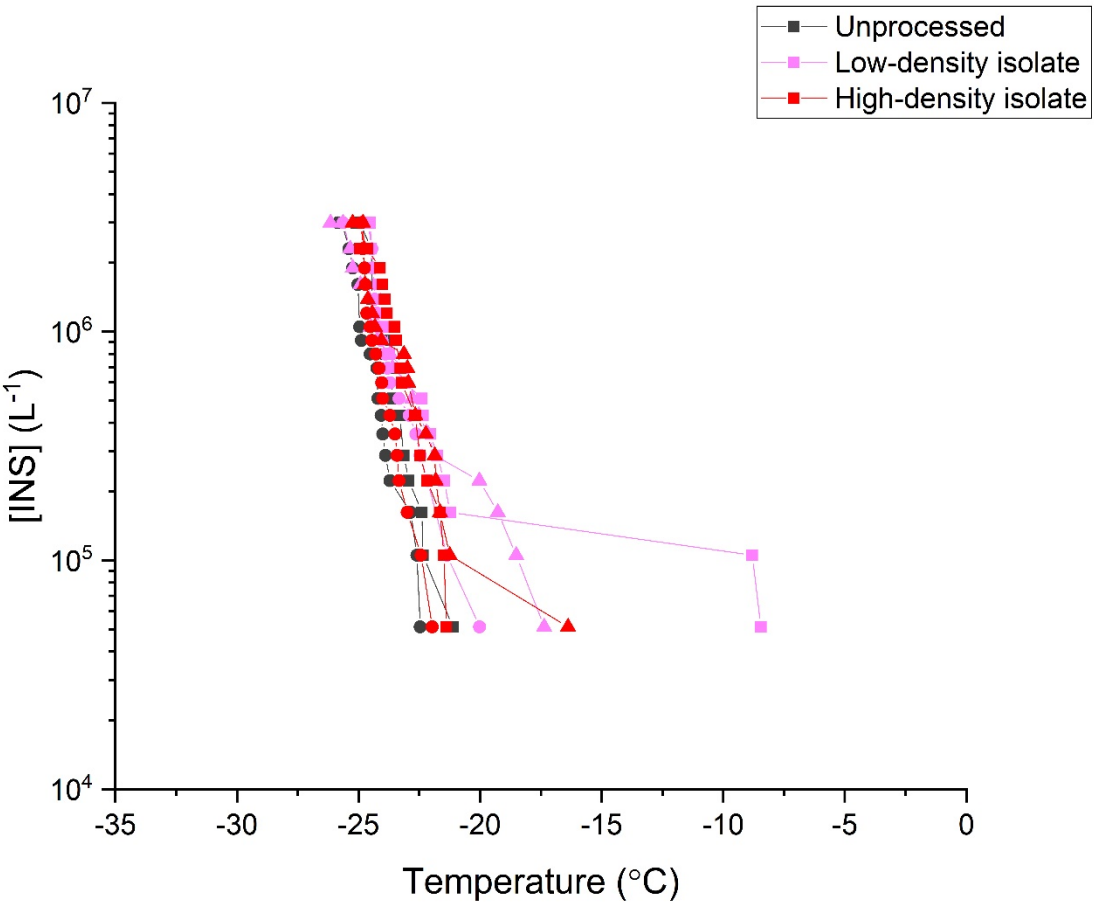

Figure 2. INS concentrations before and after density gradient centrifugation of ultrapure water. The concentration of INSs per liter of solution $[INS(T)]$ (L^{-1}) is shown for each unprocessed ultrapure water (black), low-density isolate (pink), high-density isolate (red), and ultrapure water control (grey). Different shapes represent different experimental replicates. All freezing temperatures have been corrected for freezing point depression from added KNO_3 (0.0186 °C).

https://doi.org/10.26434/chemrxiv-2024-x8t26-v2 **ORCID:** https://orcid.org/0000-0002-5621-2323

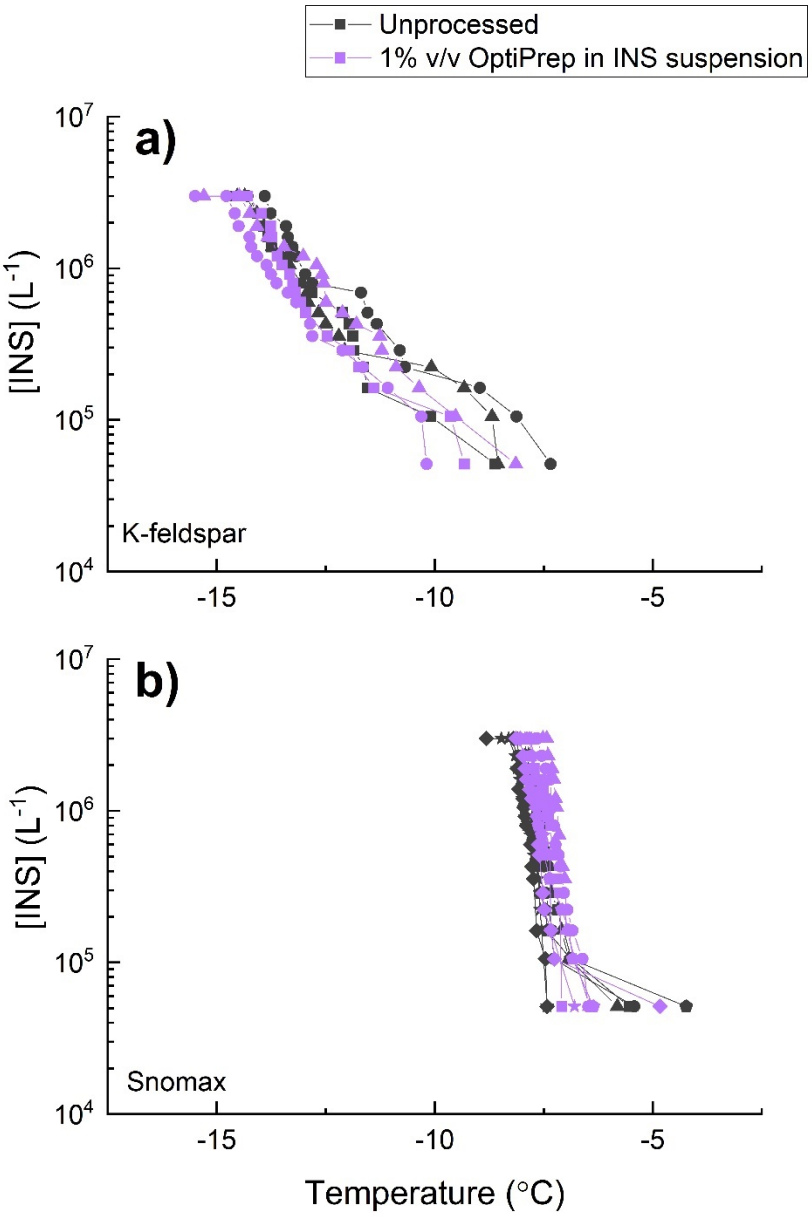

Figure 3. Impacts of added OptiPrep™ on the freezing behavior of **(a)** K-feldspar and **(b)** Snomax INS suspensions. The concentration of INSs per liter of solution $[INS(T)]$ (L^{-1}) is shown for each unprocessed sample with no OptiPrep™ added (black) and 1% v/v OptiPrep™ in standard INS suspension (purple). Different shapes represent different experimental replicates. All freezing temperatures have been corrected for freezing point depression from added KNO_3 (0.0186 °C) and OptiPrep™ (0.0036 °C).

https://doi.org/10.26434/chemrxiv-2024-x8t26-v2 **ORCID:** https://orcid.org/0000-0002-5621-2323

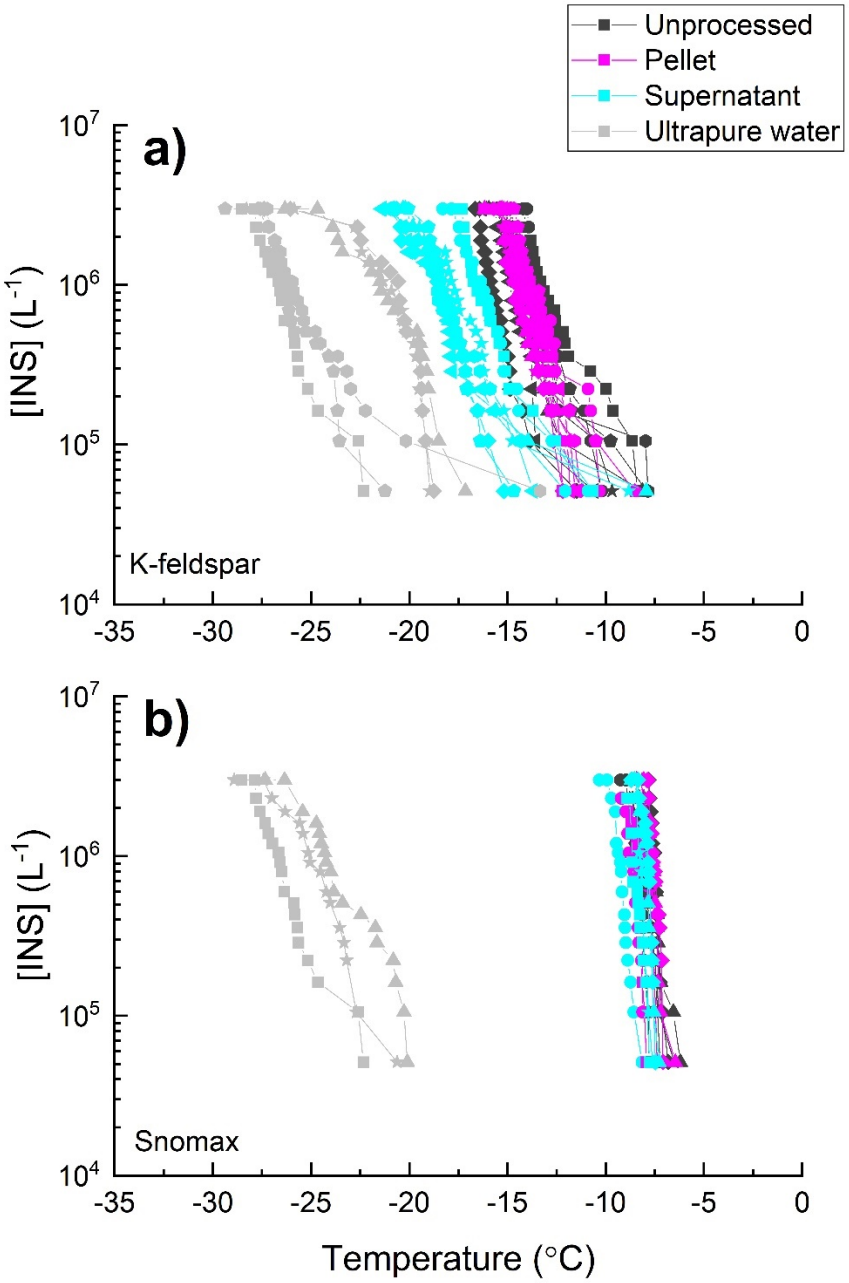

Figure 4. INS concentrations before and after washing **(a)** K-feldspar and **(b)** Snomax INS suspensions via differential centrifugation. The concentration of INSs per liter of solution $[INS(T)]$ (L^{-1}) is shown for each unprocessed INS suspension (black), resuspended centrifugal wash pellet (magenta), supernatant (cyan), and ultrapure water control (grey). Different shapes represent different experimental replicates. Ultrapure water controls correspond to the same ultrapure water used to resuspend the wash pellets. During density gradient centrifugation the resuspended centrifugal wash pellets are kept as the low- and high-density isolate and the supernatants are discarded. All freezing temperatures have been corrected for freezing point depression from added KNO_3 (0.0186 °C).

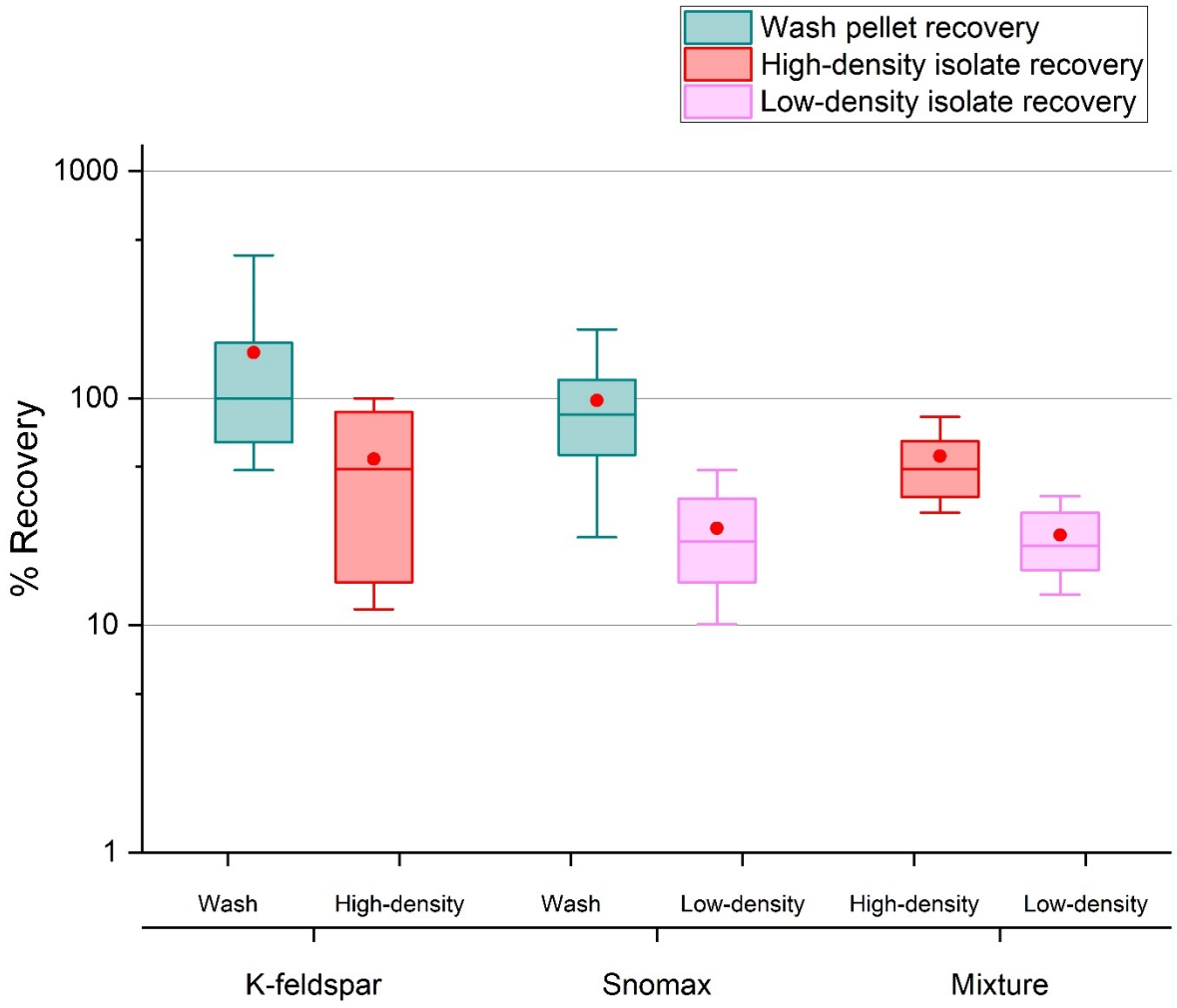

Figure 5. Summary of % recovery values for centrifugal wash experiments (cyan) and density gradient centrifugation experiments (pink for low-density isolate recoveries and red for high-density isolate recoveries) for K-feldspar, Snomax, and a K-feldspar-Snomax mixture. Red circular dots represent the mean % recovery, the center of the box represents the median % recovery, the ends of the box represent the 25th and 75th percentile of % recovery values, and the whiskers represent the 10th and 90th percentile of percent recovery values.

https://doi.org/10.26434/chemrxiv-2024-x8t26-v2 **ORCID:** https://orcid.org/0000-0002-5621-2323

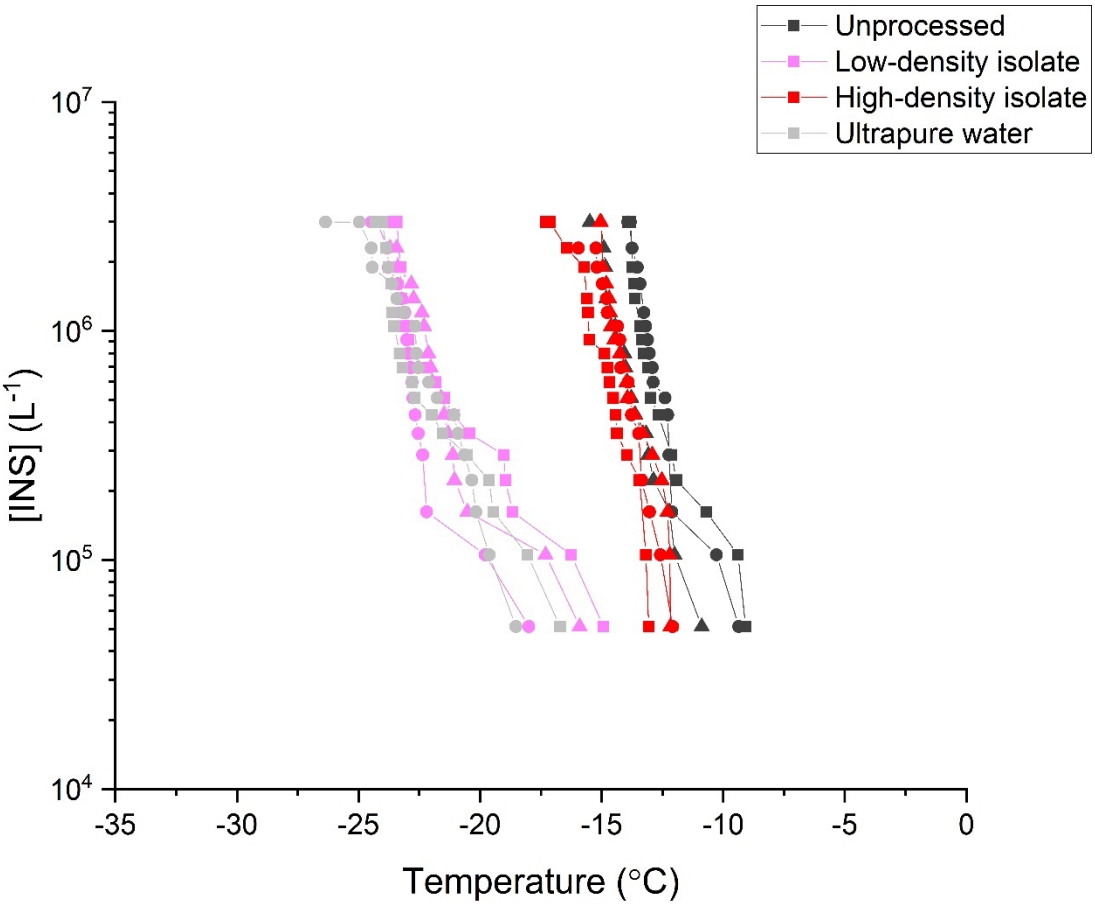

Figure 6. INS concentrations before and after density gradient centrifugation of K-feldspar. The concentration of INSs per liter of solution $[INS(T)]$ (L^{-1}) is shown for each unprocessed INS suspension (black), low-density isolate (pink), high-density isolate (red), and ultrapure water control (grey). Different shapes represent different experimental replicates. Ultrapure water controls correspond to the same ultrapure water used to resuspend the high- and low-density isolates. All freezing temperatures have been corrected for freezing point depression from added KNO_3 (0.0186 °C).

https://doi.org/10.26434/chemrxiv-2024-x8t26-v2 **ORCID:** https://orcid.org/0000-0002-5621-2323

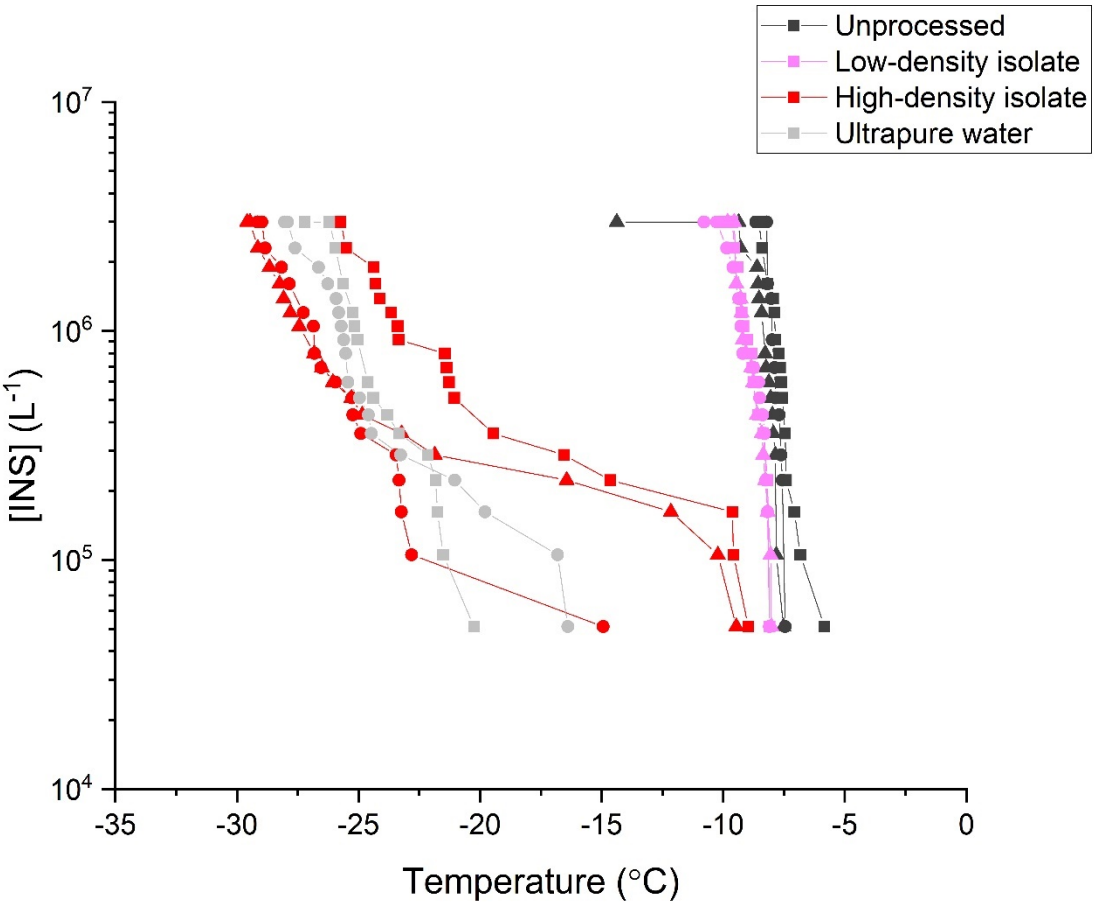

Figure 7. INS concentrations before and after density gradient centrifugation of Snomax. The concentration of INSs per liter of solution $[INS(T)]$ (L^{-1}) is shown for each unprocessed INS suspension (black), low-density isolate (pink), high-density isolate (red), and ultrapure water control (grey). Different shapes represent different experimental replicates. Ultrapure water controls correspond to the same ultrapure water used to resuspend the high- and low-density isolates. All freezing temperatures have been corrected for freezing point depression from added KNO_3 (0.0186 °C).

https://doi.org/10.26434/chemrxiv-2024-x8t26-v2 **ORCID:** https://orcid.org/0000-0002-5621-2323

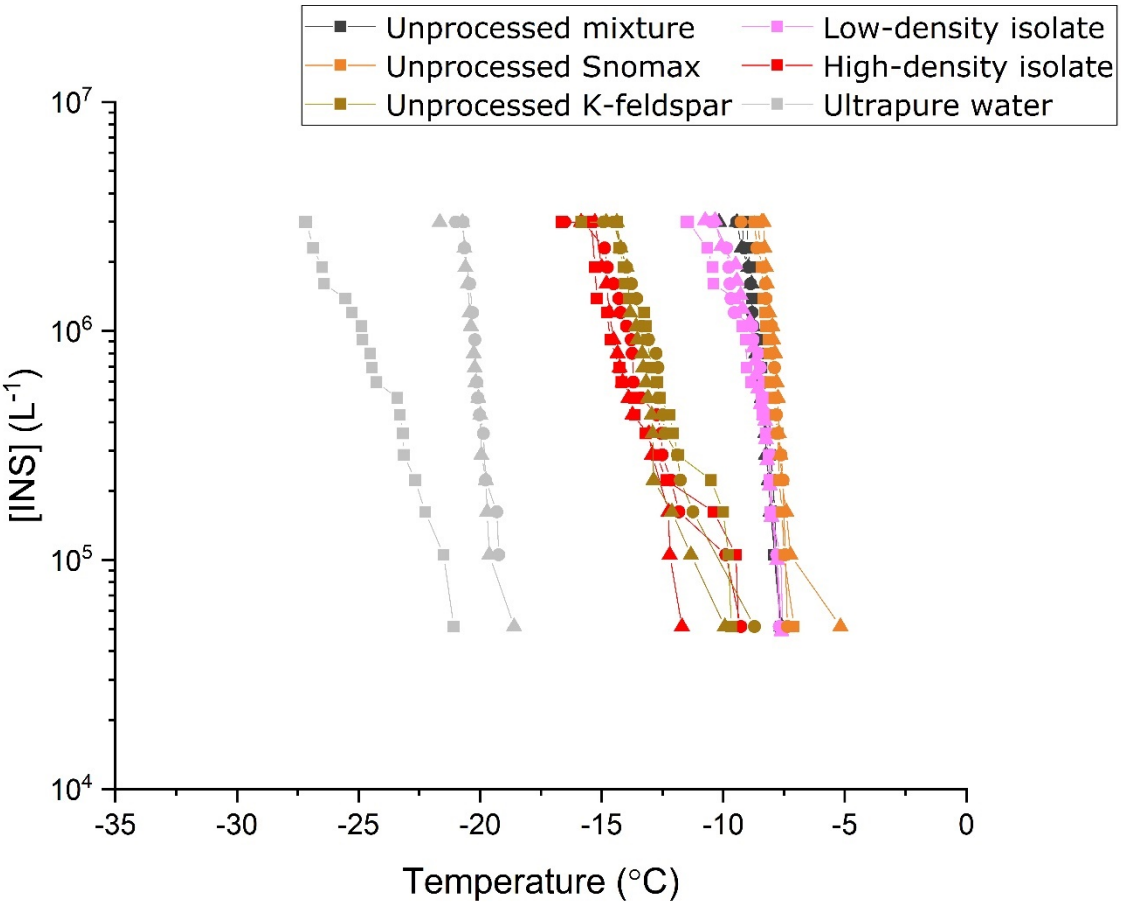

Figure 8. INS concentrations before and after density gradient centrifugation of a K-feldspar and Snomax mixture. The concentration of INSs per liter of solution $[INS(T)]$ (L^{-1}) is shown for each unprocessed INS mixture suspension (black), unprocessed Snomax suspension (orange), unprocessed K-feldspar suspension (brown), low-density isolate (pink), high-density isolate (red), and ultrapure water control (grey). Different shapes represent different experimental replicates. Ultrapure water controls correspond to the same ultrapure water used to resuspend the high- and low-density isolates. All freezing temperatures have been corrected for freezing point depression from added KNO_3 (0.0186 °C).

Captions

Figure 1. Schematic of the density gradient centrifugation procedure illustrating density gradient centrifugation (steps 1-2), isolation of the low-density material and high-density pellet (steps 3-4), and the washing step (steps 5-7) to

remove excess water-soluble density gradient medium, resulting in the finalized low- and high-density isolates for droplet freezing experiments.

Figure 2. INS concentrations before and after density gradient centrifugation of ultrapure water. The concentration of INSs per liter of solution $[INS(T)]$ (L^{-1}) is shown for each unprocessed ultrapure water (black), low-density isolate (pink), high-density isolate (red), and ultrapure water control (grey). Different shapes represent different experimental replicates. All freezing temperatures have been corrected for freezing point depression from added KNO_3 (0.0186 °C).

Figure 3. Impacts of added OptiPrep™ on the freezing behavior of **(a)** K-feldspar and **(b)** Snomax INS suspensions. The concentration of INSs per liter of solution $[INS(T)]$ (L^{-1}) is shown for each unprocessed sample with no OptiPrep™ added (black) and 1% v/v OptiPrep™ in standard INS suspension (purple). Different shapes represent different experimental replicates. All freezing temperatures have been corrected for freezing point depression from added KNO_3 (0.0186 °C) and OptiPrep™ (0.0036 °C).

Figure 4. INS concentrations before and after washing **(a)** K-feldspar and **(b)** Snomax INS suspensions via differential centrifugation. The concentration of INSs per liter of solution $[INS(T)]$ (L^{-1}) is shown for each unprocessed INS suspension (black), resuspended centrifugal wash pellet (magenta), supernatant (cyan), and ultrapure water control (grey). Different shapes represent different experimental replicates. Ultrapure water controls correspond to the same ultrapure water used to resuspend the wash pellets. During density gradient centrifugation the resuspended centrifugal wash pellets are kept as the low- and high-density isolate and the supernatants are discarded. All freezing temperatures have been corrected for freezing point depression from added KNO_3 (0.0186 °C).

Figure 5. Summary of % recovery values for centrifugal wash experiments (cyan) and density gradient centrifugation experiments (pink for low-density isolate recoveries and red for high-density isolate recoveries) for K-feldspar, Snomax, and a K-feldspar-Snomax mixture. Red circular dots represent the mean % recovery, the center of the box represents the median % recovery, the ends of the box represent the 25^{th} and 75^{th} percentile of % recovery values, and the whiskers represent the 10^{th} and 90^{th} percentile of percent recovery values.

Figure 6. INS concentrations before and after density gradient centrifugation of K-feldspar. The concentration of INSs per liter of solution $[INS(T)]$ (L^{-1}) is shown for each unprocessed INS suspension (black), low-density isolate (pink), high-density isolate (red), and ultrapure water control (grey). Different shapes represent different experimental replicates. Ultrapure water controls correspond to the same ultrapure water used to resuspend the high- and low-

density isolates. All freezing temperatures have been corrected for freezing point depression from added KNO_3 (0.0186 °C).

Figure 7. INS concentrations before and after density gradient centrifugation of Snomax. The concentration of INSs per liter of solution $[INS(T)]$ (L^{-1}) is shown for each unprocessed INS suspension (black), low-density isolate (pink), high-density isolate (red), and ultrapure water control (grey). Different shapes represent different experimental replicates. Ultrapure water controls correspond to the same ultrapure water used to resuspend the high- and low-density isolates. All freezing temperatures have been corrected for freezing point depression from added KNO_3 (0.0186 °C).

Figure 8. INS concentrations before and after density gradient centrifugation of a K-feldspar and Snomax mixture. The concentration of INSs per liter of solution $[INS(T)]$ (L^{-1}) is shown for each unprocessed INS mixture suspension (black), unprocessed Snomax suspension (orange), unprocessed K-feldspar suspension (brown), low-density isolate (pink), high-density isolate (red), and ultrapure water control (grey). Different shapes represent different experimental replicates. Ultrapure water controls correspond to the same ultrapure water used to resuspend the high- and low-density isolates. All freezing temperatures have been corrected for freezing point depression from added KNO_3 (0.0186 °C).